scientific reports

Check for updates

OPEN

Thermal effects and ephaptic entrainment in Hodgkin–Huxley model

Matheus Phellipe Brasil de Sousa[1,3], Gabriel Moreno Cunha[1,3], Gilberto Corso[1,2] & Gustavo Zampier dos Santos Lima[1,2,3,4]✉

The brain is understood as an intricate biological system composed of numerous elements. It is susceptible to various physical and chemical influences, including temperature. The literature extensively explores the conditions that influence synapses in the context of cellular communication. However, the understanding of how the brain's global physical conditions can modulate ephaptic communication remains limited due to the poorly understood nature of ephapticity. This study proposes an adaptation of the Hodgkin and Huxley (HH) model to investigate the effects of ephaptic entrainment in response to thermal changes (HH-E). The analysis focuses on two distinct neuronal regimes: subthreshold and suprathreshold. In the subthreshold regime, circular statistics are used to demonstrate the dependence of phase differences with temperature. In the suprathreshold regime, the Inter-Spike Interval are employed to estimate phase preferences and changes in the spiking pattern. Temperature influences the model's ephaptic interactions and can modify its preferences for spiking frequency, with the direction of this change depending on specific model conditions and the temperature range under consideration. Furthermore, temperature enhance the anti-phase differences relationship between spikes and the external ephaptic signal. In the suprathreshold regime, ephaptic entrainment is also influenced by temperature, especially at low frequencies. This study reveals the susceptibility of ephaptic entrainment to temperature variations in both subthreshold and suprathreshold regimes and discusses the importance of ephaptic communication in the contexts where temperature may plays a significant role in neural physiology, such as inflammatory processes, fever, and epileptic seizures.

In the central nervous system, various structures play crucial roles in receiving and transmitting information across different levels[1]. These diverse levels of neuronal communication within the brain initiate intricate cognitive processing mechanisms essential for functions like memory and consciousness[2,3]. Neurons, vital components in this context, are responsible for processing and relaying signals[4,5]. Organized in interconnected groups, neurons contribute to the nervous system's capacity to adapt and perform various functions in a coordinated and efficient manner[4,6]. While neuronal communication typically occurs through synapses, it is noteworthy that neuronal activity generates electrical fields that propagate in the extracellular environment, exerting a modulatory influence on adjacent neurons beyond chemical synapses[7–9]. The examination of interactions between neurons, whether via synapses or electrical fields, aids in understanding the intricate brain mechanisms governing neural phenomena. Investigating these processes is indispensable for unraveling the underlying mechanisms of brain complexity, providing valuable insights for advancements in understanding and treating complex neurological conditions.

In recent decades, the impact of electrical fields on neuronal communication has been the focus of studies[10–15]. Ephaptic communication, known as communication through electric fields, may originate from a single neuron or a group of neurons[8,10,11,16]. Ephaptic neuronal communication, characterized by electrical field interactions between adjacent nerve cells, underscores an interconnection beyond traditional synapses and enhances our understanding of brain communication in the formation of memory and consciousness[9,17,18]. The impact of ephaptic communication on neurophysiological brain functions is a subject of rigorous investigation. Hypotheses

[1]Departamento de Física Teórica e Experimental, Universidade Federal do Rio Grande do Norte, Natal, RN 59078-970, Brazil. [2]Departamento de Biofísica e Farmacologia, Universidade Federal do Rio Grande do Norte, Natal, RN 59078-970, Brazil. [3]Laboratório de Simulação e Modelagem Neurodinâmica, Universidade Federal do Rio Grande do Norte, Natal, RN 59078-970, Brazil. [4]Escola de Ciências e Tecnologia, Universidade Federal do Rio Grande do Norte, Natal, RN 59078-970, Brazil. ✉email: gustavo.zampier@ufrn.br

suggesting that ephaptic communication acts not only as an epiphenomenon-merely a consequence or noise effect of neuronal activity-but also as a causative form of communication influencing neuronal dynamics have been proposed[9,10,15–17]. Research indicates that while the stimulation caused by an external electric field from one neuron may not suffice to trigger action potentials in another, ephaptic fields can modulate and affect action potential synchronization[10,11,19,20].

Temperature is widely acknowledged as one of the most influential environmental factors affecting animal physiology[21]. Although further exploration is needed, the impact of temperature on neuronal activity is critical, leading to modifications in the frequency of neuron action potentials[21–24]. Temperature fluctuations influence the activation and inactivation of several ion channels, including voltage-dependent K^+, Na^+, and Ca^{2+} channels, thereby affecting the generation of action potentials[25–28]. Notably, elevated temperatures consistently increase firing frequency[29] and decrease the duration of action potentials[30]. Furthermore, it is well-documented that the rates of biochemical reactions in organisms vary with temperature, impacting the functionality of enzymes and proteins crucial to neuronal dynamics[23,24,31,32]. Consequently, thermal factors are intricately associated with conformational changes in ion channels[32,33]. The interplay between neural stimulation properties and temperature has been an actively researched area since pioneering electrophysiological investigations, with outcomes aligning with theoretical predictions based on the Hodgkin–Huxley model[27,34–36].

On the other hand, research on conformational changes in ion channels and neuronal dynamics has primarily focused on synaptic communication, overlooking ephaptic interactions influenced by temperature. This gap highlights the need for further investigation[37]. Consequently, this study explores the impact of thermal variations on ephaptic communication. Initially, in the subthreshold regime, we follow an analogous approach to empirical studies[38] and hybrid model simulations[11], obtaining similar results for phase differences. Subsequently, we introduce the thermal factor ΔT_{10}, dependent on temperature (Arrhenius's function)[39,40], thereby expanding the phenomenology of the Hodgkin and Huxley model to incorporate thermal modifications. The simulations conducted in this study explore the intricate interactions between ephaptic and thermal influences.

The remainder of this paper is structured as follows: the next section details the primary methodologies used to analyze the results, including circular statistics and inter-spike interval (ISI). Following this, the Results section presents the data obtained from the simulations, classified into two regimes: Subthreshold and Suprathreshold. Finally, the concluding section offers a comprehensive discussion of the study's findings, emphasizing implications for functionality and effectiveness, and outlining potential avenues for future research.

Hodgkin–Huxley model

The Hodgkin–Huxley model[24,41–43] is the most renowned conductance-based model that quantitatively describes the propagation of action potentials across neuronal membranes. This model incorporates three pivotal ionic currents crucial for action potential generation. The complete set of Hodgkin–Huxley equations governing membrane potential dynamics is given by:

$$C_m \frac{dV_m(t)}{dt} = I(t) - I_{Na} - I_K - I_L \tag{1}$$

Here, C_m denotes membrane capacitance, and $I(t)$ represents the applied current. The sodium current is expressed as $I_{Na} = g_{Na} m^3 h (V_m - V_{Na})$, predominant during membrane depolarization, modulated by activation (m) and inactivation (h) variables. The potassium current, contributing to membrane re-polarization, is represented by $I_K = g_k n^4 (V_m - V_K)$, governed by the activation variable n. The "leak" current $I_L = g_L (V_m - V_L)$ accounts for additional ionic influences not explicitly modeled. Constants g_{Na}, g_K, and g_L represent conductance for sodium, potassium, and leak channels respectively, while V_{Na}, V_K, and V_L denote Nernst potentials. The dynamics of gating variables (n, m, h), also known as gating variables, are described by first-order differential equations:

$$\frac{dx}{dt} = \phi_i(\Delta T)(\alpha_x(V_m)(1 - x) + \beta_x(V_m)x) \quad (\text{for } x = n, m, h) \tag{2}$$

Here, $\alpha_x(V_m)$ and $\beta_x(V_m)$ are rate constants dependent on membrane potential V_m, crucial for transitioning between closed and open states of ion channels[41]. Specifically, for n: $\alpha_n(V_m) = 0.01 \frac{10 - V_m}{e^{(\frac{10 - V_m}{10})} - 1}$ and $\beta_n(V_m) = 0.125 e^{(-\frac{V_m}{80})}$; for m: $\alpha_m(V_m) = 0.1 \frac{25 - V_m}{e^{(\frac{25 - V_m}{10})} - 1}$ and $\beta_m(V_m) = 4 e^{(-\frac{V_m}{18})}$; and for h: $\alpha_h(V_m) = 0.07 e^{(-\frac{V_m}{20})}$ and $\beta_h(V_m) = \frac{1}{e^{(\frac{30 - V_m}{10})} + 1}$. The thermal factor $\phi_i(\Delta T)$ in Eq. (2) is defined as:

$$\phi_i(\Delta T) = Q_{10}^{\Delta T_{10}} \tag{3}$$

for $i = \{Na^+, k^+\}$, indicating thermal factor changing according to considered ion channel, as will be discussed later in the text. Futhermore, $\Delta T_{10} = (T_2 - T_1)/10$ (°C) represents the temperature difference, with T_1 as the base or reference temperature ($T_1 = 6.2$ °C), and T_2 the test temperature[39,40]. This factor modulates the kinetics of ion channel gating variables, integrating thermal effects into the Hodgkin-Huxley model's phenomenology.

Ephaptic entrainment in Hodgkin–Huxley model

Ephaptic neuronal coupling describes a phenomenon where the electric field generated by neuronal firing influences nearby neurons or electric sources[44,45] (see Fig. 1). This electric field can induce an ionic current following Ohm's law, directly impacting the membrane potential and spike timing of adjacent neurons[11,38]. Empirical studies by Anastassiou et al.[38] and numerical simulations by Cunha et al.[11,46] have demonstrated that while the electrical interaction between neighboring neurons is up to 1000 times weaker than synaptic interactions, it can still modulate neuronal communication[16,47]. This subtle electrophysiological mechanism underscores the

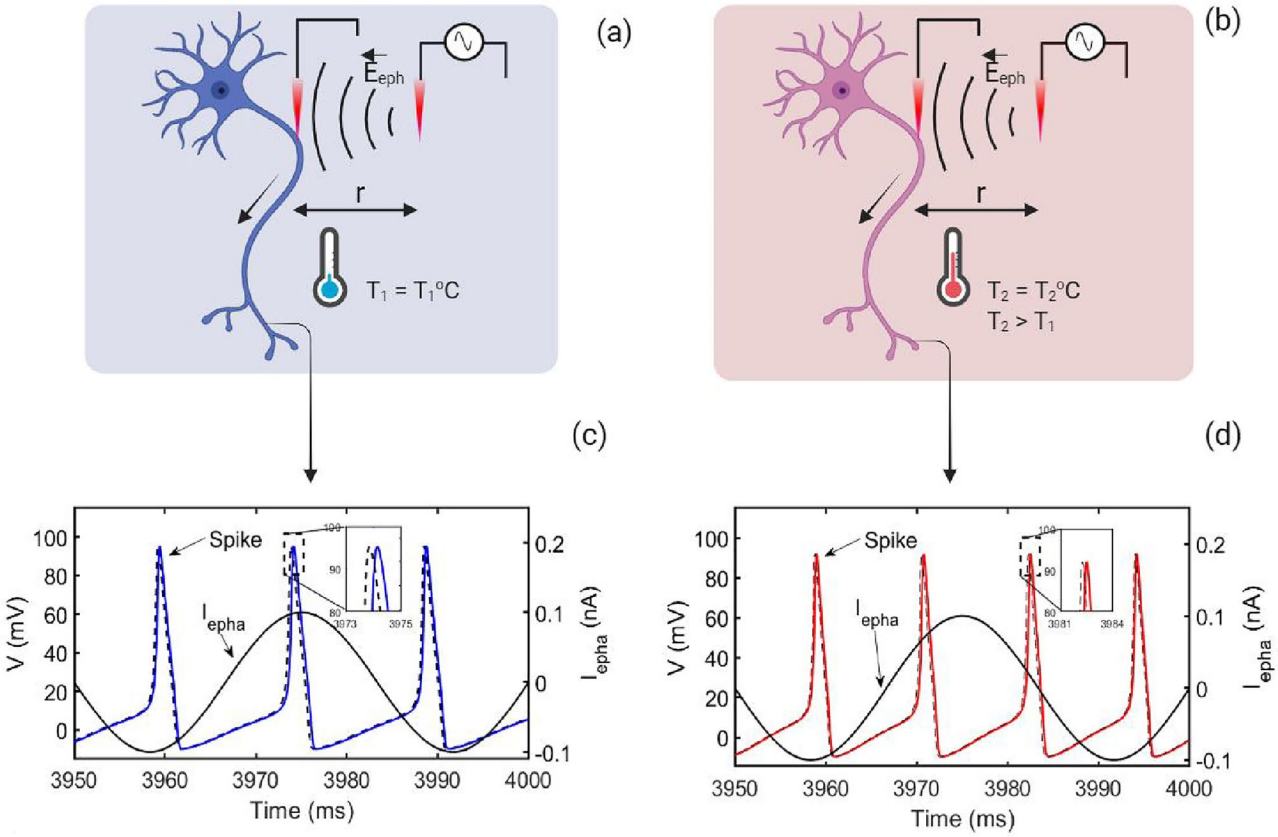

Figure 1. Thermal effects of the ephaptic model on firing frequency preferences: (**a**) schematic illustration of a neuron positioned far from the source electrode (Local Field Potential—LFP) at a distance r and temperature T_1, subjected to the LFP oscillating electric field (ephaptic field—E_{eph}). (**b**) Represents the neuron at the same distance r from the LFP but at a temperature T_2, for ($T_2 > T_1$). (**c**) Firing pattern of the neuron at temperature T_1 (blue line) in the presence of the ephaptic signal ($I_{epha}(nA)$) from the LFP (black line). The dashed line represents the neuronal firing under the same conditions but without the ephaptic signal (LFP off). The highlighted box in the panel shows entrainment due to the ephaptic signal, shifting ephaptic firing relative to firing in the absence of the ephaptic signal (dashed black line). In (**d**), it is shown that increasing the temperature from T_1 to T_2 increases the firing rate (red line). The ephaptic signal (solid black line) is represented here as a current signal.

complexity and inter-connectivity of neural activities, revealing the sophisticated regulation and communication inherent in the nervous system.

In this context, following established methodologies (Holt and Koch[48]; Goldwyn and Rinzel[49]), we rewrite the differential Eq. (1), governing the dynamics of the neuron's membrane potential receiving an oscillatory electric field from a source (LFP). We decompose the injected current $I(t)$ as $I(t) \approx I_0 + I_0^{'}(t)$, where $I_0^{'}(t)$ represents the disturbance term from the ephaptic field (LFP oscillation's source electrode), and I_0 is a constant current term. To assess the ephaptic influence on neuronal potential, we consider a spherical electrode in the extracellular environment. The potential induced by the injected current from the extracellular electrode follows Holt and Koch's proposal[48], which has been applied in subsequent studies[10,11,46]. The expression for the extracellular electrical potential is given by $V_{epha}^{ext} = \frac{\rho}{4\pi r} I_{ext}(t)$, where ρ is the resistivity of the extracellular medium, and r is the distance between the source and the measurement point (neuron).

Assuming the ohmic membrane hypothesis, at each time instant, the external potential (induced by an external electric field) can be expressed as $V_{epha}^{int} - \frac{\rho}{4\pi r} I_{ext}(t) = \frac{I_0^{'}(t)}{G_{eq}}$. Therefore, considering the grounded brain hypothesis[50], we assume $V_{epha}^{int} = 0$, allowing us to express the ephaptic current as:

$$I_0^{'}(t) = -\frac{\rho}{4\pi r} G_{eq} I_{ext}(t) \tag{4}$$

Moreover, using the association of resistors in parallel for the model circuit, the maximum equivalent conductance can be defined as $G_{eq} = g_{Na} + g_K + g_L$.

Following the approach of other works on ephaptic drag[10,11,46], the used ephaptic term is sinusoidal, $I_{ext}(t) = Asin(2\pi ft)$. Therefore, the equation for the membrane potential is given by:

$$C_m \frac{dV_m}{dt} = I_0 - g_{Na} m^3 h(V_m - V_{Na}) - g_k n^4 (V_m - V_K) - g_L (V_m - V_L) - I_{epha} sin(2\pi f t) \quad (5)$$

where the constants $\frac{\rho}{4\pi r} G_{eq} A$ is summarized in I_{epha}. The new constant I_{epha} represents the intensity of the ephaptic current in the model.

Considering the new Hodgkin–Huxley model with ephaptic term, in the following we study how certain values of frequency f the thermal factor $Q_{10}(T)$, modulate the ephaptic entrainment phenomenon. Values of frequency and ephaptic amplitude were taken according to studies[11,16], as shown in Table 1. Figure 1c,d depict how ephaptic influences, albeit significantly weaker, can still modulate the peak of neuronal firing, highlighting the modulatory characteristic of ephaptic and thermal effects.

Thermal effects through the factor $\phi(T)$ using Arrhenius Q_{10} function

A crucial aspect of the Hodgkin–Huxley model lies in the incorporation of thermal effects through the factor $\phi(T)$, which introduces the temperature sensitivity of ion channel kinetics. The function $\phi(T)$, provided by Eq. (3), includes a factor Q_{10} that relates to the temperature's impact on the opening and closing processes of the channel. The Q_{10} factor quantifies the ratio between the rates of a biochemical reaction occurring at temperatures differing by 10 °C. Furthermore, the thermal factor Q_{10} serves as a measure of temperature influence on ionic channel conductance dynamics. High temperatures enhance biological processes by providing additional energy for chemical reactions. Therefore, the Q_{10} factor is commonly used in neuroscience to adjust the reaction rates of voltage-activated membrane conductance's at different temperatures, but it is still widely considered constant[51]. On the other hand, several studies have shown an inverse relationship between temperature and the Q_{10} factor. In other words, when the temperature increases, the Q_{10} factor gradually decreases[27,51–54].

Considering the previous explanation and with experimental data providing approximate values of Q_{10} in specific temperature ranges, the present work incorporates a temperature-dependent Q_{10} function based on Arrhenius theory[55]. Moreover, according to Pahlavan et al. approach[54], the rate coefficient is defined by:

$$k^{Arr}(T) = Be^{-\frac{E_a}{RT}} \quad (6)$$

where k^{Arr} is the Arrhenius's reaction rate constant, B is the pre-exponential factor or constant frequency factor, E_a the activation energy or energy barrier independent of temperature, R the universal gas constant and T is the temperature measured in Kelvin. Using transition state theory[56], the relationship is $k^{tr}(T) = (K_B T/h)e^{-\Delta G/RT}$, where K_B and h are the Boltzmann's and Planck's constants, respectively, and ΔG is the free energy of the activation barrier that is related to the enthalpy (ΔH) and the entropy (ΔS) as: $\Delta G = \Delta H - T\Delta S$. Thus, by substituting this expression into the k^{tr} equation we have: $k^{tr}(T) = ((k_B T/h)e^{\Delta S/R})e^{-\Delta H/RT}$. Therefore, using the Q_{10} definition as $Q_{10} = (k(T_2)/k(T_1))^{10/(T_2-T_1)}$, where $k(T_1)$ and $k(T_2)$ are rate coefficients at two different temperatures T_1 and T_2, and using the Arrhenius equations, the Q_{10} can be rewrite as: $Q_{10}^{Arr} = e^{10E_a/(RT(T+10))}$, or applying the transition rate theory:

$$Q_{10}^{tr} = e^{\frac{10\Delta G}{RT(T+10)}} \quad (7)$$

The values of ΔG for the specific ions channels were based on Table 1 of Pahlavan et al. study (2023)[54]. For Na^+ ion channels the $\Delta G = 86.26 \pm 4.42$ (kJ mol^{-1}) and for the K^+ ion channel we considered $\Delta G = 97.96 \pm 7.13$ (kJ mol^{-1}). In this paper, we observed that $Q_{10}(T)$ behavior is analogous to the Hodgkin and Katz study[51] from the temperature range $[0 - 20]$ °C (see Fig. 2. Using the equation 3 we calculated $Q_{10}(T)$ for distinct temperature intervals for sodium and potassium conductance. The Arrhenius approach $Q_{10}(T)$ is plotted in Fig. 2.

The T_1 temperature value is equal 6.2 °C[51] ($T_1 = 6.2$ °C). Furthermore, the Fig. 2 shows the behavior of Q_{10} for sodium and potassium conductance.

Statistical tools

For the statistical analysis in this study, we employed common tools widely utilized in the field of neuroscience, such as circular statistics, population vectors, and the Inter-Spike Interval (*ISI*).

Circular statistic and population vector

Circular statistics is a specialized branch of statistics dedicated to analyzing angular datasets[57]. A key principle in circular statistics is the treatment of angles where 0° and 360° are equivalent. In this study, circular statistics were employed in two main contexts. Firstly, in the subthreshold state of neurons, they were used to assess phase discrepancies between subthreshold neuronal potentials and ephaptic signals. Secondly, in the suprathreshold state, circular histograms were generated to reveal preferred phases of ephaptic signal occurrences relative to neuronal potentials. These analyses utilized the MATLAB toolbox "CircStat"[58]. Additionally, the population vector method[59,60] was employed in the suprathreshold state to determine phase preferences between neuronal potentials and ephaptic field signals.

Hilbert transform

The Hilbert transform, $\mathscr{H}$, is a useful mathematical tool in signal analysis[11,38,61]. This tool generates the instantaneous phase signal, applying $\mathscr{H}$ to a time series $x(t)$ provides a new transformed signal $X(t) = \mathscr{H}(x(t))$, which is in time domain. The original time series and the transformed signal composed an analytic signal: $x_{ana}(t) = x(t) + iX(t)$. In addition, the instantaneous phase can be obtained as follows: $\phi(t) = arct(X(t)/x(t))$.

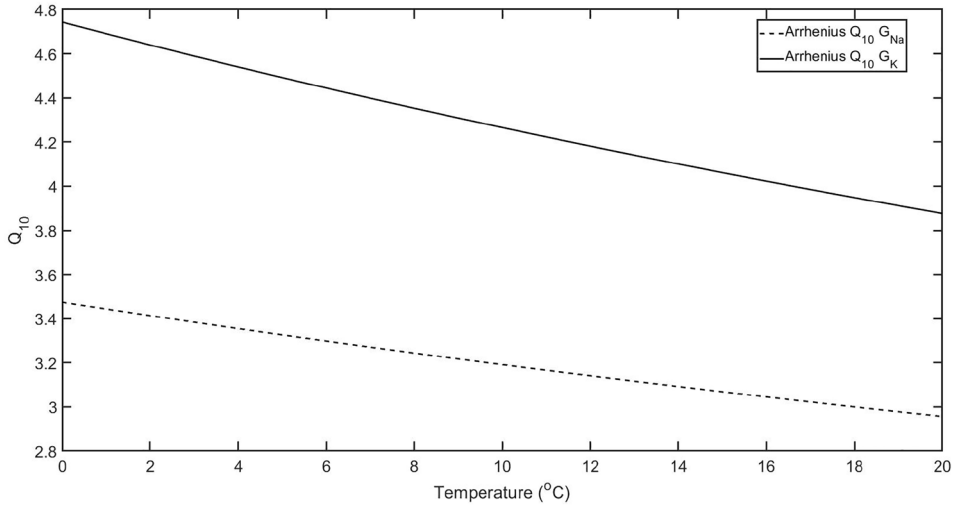

Figure 2. Thermal factor variation with temperature following Arrhenius model. The figure shows the behavior of $Q_{10}(T)$ as function of temperature (°C) for sodium conductance G_{Na} (black dashed line) and potassium conductance G_K (black continuous line).

Constants	Values
I_{epha}	100 nA
C_m	1 µF
g_{Na}	120 S/cm^2
g_K	36 S/cm^2
g_L	0.3 S/cm^2
V_{Na}	115 mV
V_K	− 12 mV
V_L	10.59 mV
V_{rest}	0 mV
ρ	3.5 Ω m
r	50 µm

Table 1. Table for the parameters used in the numerical simulations.

This tool was applied in subthreshold and suprathreshold regime to evaluate the phase difference between the membrane potential and the ephaptic signal.

Inter-spike interval

The Inter-Spike Interval (ISI)[62] is a critical tool in neuronal electrophysiology, used to measure the time durations between successive action potential spikes. This analytical method enables the exploration of dynamic neuronal activity patterns and behavioral characteristics. ISI analysis has illuminated various dynamic properties of neuronal behavior[63,64], offering valuable insights into neurological aspects[65–67]. Estimating ISI serves as a pivotal approach for understanding diverse behaviors arising from interactions between electric fields and neurons. Furthermore, ISI analysis contributes to uncovering the impact of ephaptic interactions on neuronal coupling[65].

Results

In this study, we employed a modified Hodgkin–Huxley model that incorporates ephaptic entrainment to investigate the thermal effects across various temperature values, incorporating the Arrhenius's thermal function. The results are categorized into two distinct regimes. The first regime corresponds to the subthreshold state of the neuron, where the neuron does not generate action potentials ($I_0 = 0$ or $I_0 < I_{threshold}$). The second regime represents the suprathreshold state, where the neuron is capable of eliciting action potentials ($I_0 > I_{threshold}$). These distinct dynamics provide valuable insights into neuronal behavior under different excitatory conditions.

Time series data were generated spanning a total of 60 seconds, with a time step of $dt = 10^{-3}$, excluding the initial 10 seconds to ensure system stabilization. MATLAB's fourth-order Runge-Kutta method facilitated the generation of these series. Additional fixed parameters used in the simulation are detailed in Table 1.

Subthreshold results

In Fig. 3, the results of subthreshold phase difference ($I_0 = 0$) are presented for different values of ephaptic frequency f and temperatures T. In this simulation, the frequencies was chosen as $f = [2, 8, 30]$ Hz and the ephaptic current intensity is set at $I_{epha} = 100$ nA for all results according to studies[10,11]. The blue lines in Fig. 3 correspond to the angular distribution, while the black lines display the mean angle vector, indicating both the average direction and the concentration of data around that direction.

Figure 3a shows that for $f = 2$ Hz and $T = 0$ °C, the phase difference between the subthreshold neuronal potential and the ephaptic signal is approximately $\Delta\theta = \pi$. Figure 3b reveals a phase difference closer to $\Delta\theta = \pi$ compared to Fig. 3a, but for $T = 5$ °C. In Fig. 3c, at $T = 10$ °C and $f = 2$ Hz, the phase difference is anti-phase, $\Delta\theta = \pi$. Figure 3d presents the phase difference results for $f = 8$ Hz and $T = 0$ °C, where the phase difference exceeds 200°. Figure 3e shows that at $T = 10$ °C and $f = 8$ Hz, the phase difference tends to approach $\Delta\theta = \pi$. In Fig. 3f, the phase difference is anti-phase, similar to Fig. 3c. Finally, the third row of Fig. 3 shows the behavior of subthreshold phase difference for ephaptic frequency $f = 30$ Hz at $T = 0$ °C (g), $T = 5$ °C (h), and $T = 10$ °C (i). An interesting feature observed in all panels is that the phase difference is predominantly anti-phase for all values of ephaptic frequency and temperature (see supplementary material).

Suprathreshold results

An intuitive view of the effects of temperature changes in the suprathreshold regime is shown in Fig. 4. Disregarding the ephaptic contribution ($I_{epha} = 0$), this figure illustrates the consequences of temperature changes on neuron firing rates and temporal series. The temporal series were generated for values of I_0 highlighted (the minimum current required to produce action potentials) in the figure.

Figure 4a depicts the model's firing rate profile at $T = 0$ °C as a function of the injected current I_0, ranging from 0 to 160 μA. In Fig. 4b, it can be observed that at $T = 5$ °C, the model's firing rate increases, and the suprathreshold range of I_0 decreases. Figure 4c shows that at $T = 10$ °C, the same behavior observed in Fig. 4a,b is present. Finally, Fig. 4d demonstrates that among all previously presented temperature values, at $T = 15$ °C, the model exhibits the highest firing rates and requires the shortest range of I_0 to elicit spikes in the system. Figure 4e presents the temporal series for the Hodgkin–Huxley model with a minimal injected current ($I_0 = 9$ μA) chosen to make the model fire at $T = 0$ °C. It is observed in this figure that within the interval of 0.1s, the model generates three action potentials. In Fig. 4f, the number of action potentials increases to six within the same time interval when the temperature is increased to $T = 5$ °C. Figure 4g ($T = 10$ °C) and h ($T = 15$ °C) exhibit a similar pattern of behavior as observed in Fig. 4f due to the temperature increase. Additionally, in Fig. 4e–h, the increase in temperature reduces the amplitude of action potentials, corroborating previous studies.

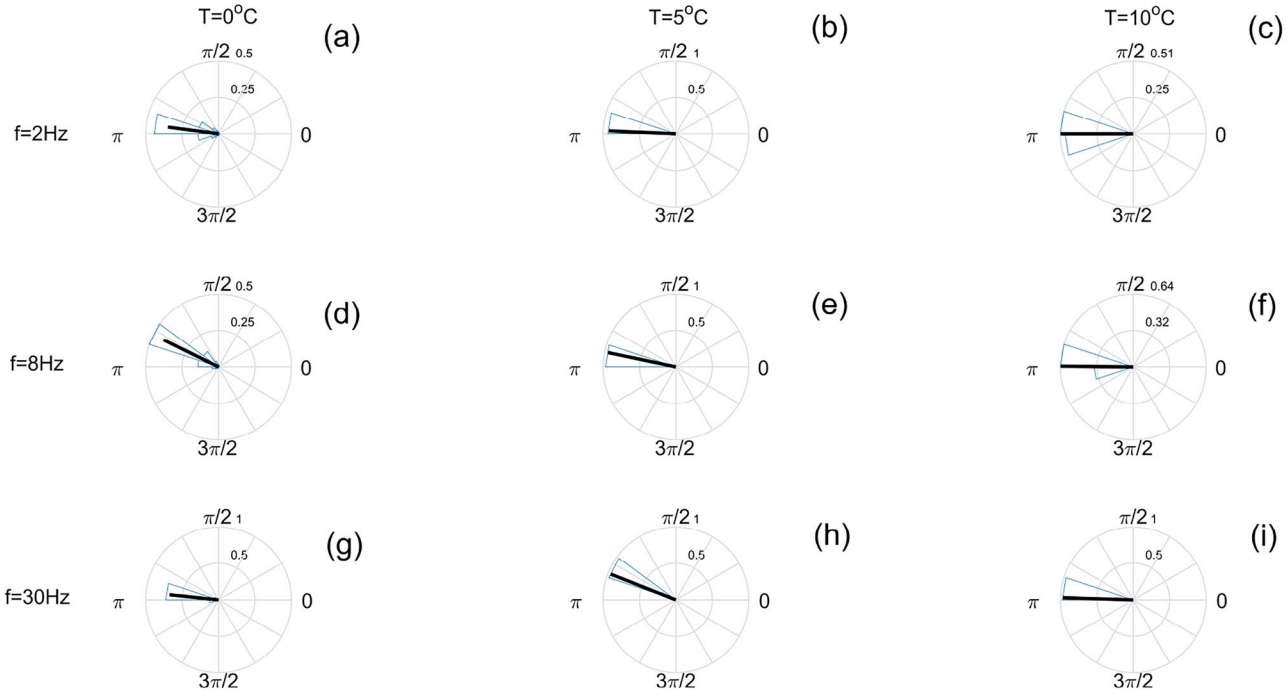

Figure 3. Subthreshold phase difference for distinct ephaptic frequencies and temperatures. The results of phase difference are changed by ephaptic signal frequency and temperature T. In this panel the frequency varies along the column and the thermal factor along the line. Setting the ephaptic current intensity at $I_{epha} = 100$ nA and the internal current applied as $I_0 = 0$, the first line shows the behavior of phase difference for 2 Hz ephaptic frequency, $T = 0$ °C (**a**), $T = 5$ °C (**b**) and $T = 10$ °C (**c**). The second line of this figure shows the phase difference results for $f = 8$ Hz for temperature: $T = 0$ °C (**d**), $T = 5$ °C (**e**) and $T = 10$ °C (**f**). The third line (**g**–**i**) shows the phase difference results for 30 Hz ephaptic frequency and the same temperatures.

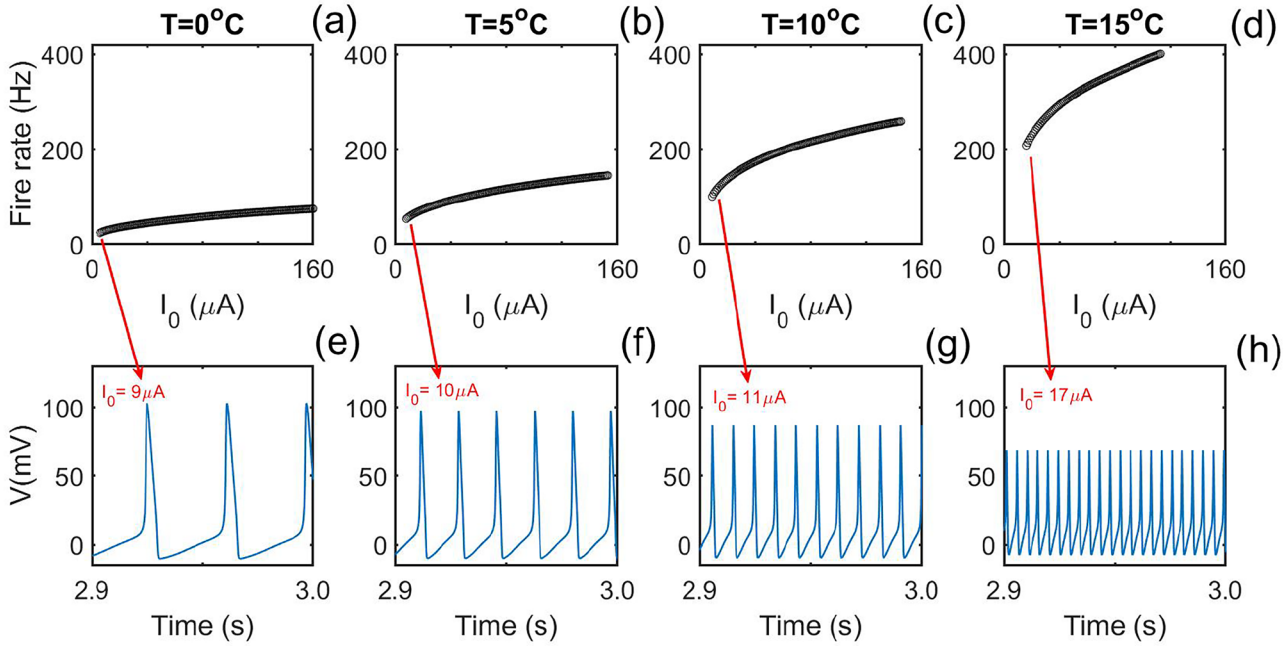

Figure 4. Temporal series and fire rate profile according to temperature (without ephaptic effect). All temporal series shown in this panel were generated with a minimum injected current I_0 (red arrow). In (**a**), the firing rate of the model versus I_0 is presented for $T = 0$ °C. In (**b**), it is shown that the firing rate increases with temperature at $T = 5$ °C. Additionally, the range of I_0 leading to firing is reduced. Panels (**c**) and (**d**) exhibit the same pattern for temperatures $T = 10$ °C and $T = 15$ °C. Panel (**e**) illustrates the action potential profile for $T = 0$ °C over a 0.1s interval with $I_0 \approx 9$ μA. It also shows an increased number of action potentials within the same interval for $T = 5$ °C, where $I_0 \approx 10$ μA. Panels (**f**) and (**g**) demonstrate similar results for $T = 10$ °C and $T = 15$ °C. The I_0 values used in these figures were 11 μA and 17 μA, as indicated by the highlighted red arrows.

In order to isolate the effects of ephaptic interactions in the system, Fig. 5 demonstrates the model's response with and without ephaptic interaction at the standard temperature $T = 6.2$. At this temperature, the thermal factor in Eq. (3) equals one, thus disregarding thermal variations.

In the absence of ephaptic interaction, Fig. 5a presents the control membrane potential time series (black dashed line) alongside the ephaptic signal (red line) over a short time interval, for injected current $I_0 = 10$ μA and ephaptic current $I_{epha} = 100$ nA. Figure 5b illustrates the scenario where ephaptic interaction ($f = 30$ Hz) occurs between the ephaptic signal and the membrane potential, for the same injected and ephaptic current intensities used in Fig. 5a, resulting in the ephaptic time series (blue line). Figure 5c compares the control membrane potential time series without ephaptic interaction to the ephaptic time series. It is observed in panel (c) that even with ephaptic interaction present, the number of action potentials remains the same as in the case without ephapticity. The unique effect observed in this panel is the shift in action potential timing between the control series and the ephaptic series.

The addition of ephaptic current ($I_{epha} \neq 0$) affects the variability of ISI, which we measure using the standard deviation of ISI. Figure 6 presents the results of ISI standard deviation (ISI_{std}) versus ephaptic signal frequency for temperature values of 0 °C, 5 °C, 10 °C, and 15 °C. For each panel, we use the minimum current I_0 at which the model fires with the lowest firing rate. The base values of I_0 were 9 μA, 10 μA, 11 μA, and 17 μA for $T = 0$ °C, 5 °C, 10 °C, and 15 °C, respectively.

Figure 6a shows the profile of ISI_{std} for $T = 0$ °C. In this case, the model exhibits a natural frequency $f_N \approx 28$ Hz. Additionally, the ISI deviation becomes zero at ephaptic frequencies equal to the resonant values (e.g., $f \approx 28$ Hz, $f \approx 56$ Hz and so on). Further, the ISI_{std} display a maximum around $f \approx 48$ Hz (best frequency preference) and then decay to zero around 200Hz. Figure 6b displays the ISI deviation for $T = 5$ °C, where the resonant frequency is $f_N = 58$ Hz. Similarly to Fig. 6a, the ISI deviation tends towards zero at resonant ephaptic frequencies. Figure 6c corresponds to $T = 10$ °C, with a resonant frequency of $f_N = 106$ Hz. Again, the ISI deviation is nearly zero at resonant frequencies, as observed in panels (Fig. 6a,b). Furthermore, Fig. 6d shows the profile of ISI_{std} for $T = 15$ °C, where the resonant frequency is $f_N = 214$ Hz. Across Fig. 6a–d, it is noted that ISI_{std} values decrease with increasing temperature.

To better understand the behavior of ISI_{std} as presented in Figs. 6, 7 illustrates how the phase difference is influenced by changes in ephaptic frequency oscillation f at $T = 0$ °C. Figure 7a,b demonstrate that at ephaptic frequency $f = 0$ Hz (absence), the phase difference distribution between membrane potential and ephaptic signal is flat, showing that without ephaptic influences, the membrane potential does not present phase preference, providing a group control to other results. This result is depicted in the histogram (Fig. 7a) and the circular plot (Fig. 7b) and corroborate with the same analysis showed in[10]. In Fig. 7c, with an ephaptic frequency of $f = 2$ Hz, the phase difference exhibits a preference around $\Delta\theta = 0°$, with additional angles spread predominantly in positive values. This behavior is similarly observed in Fig. 7e ($f = 48$ Hz). Figure 7d,f display the phase difference

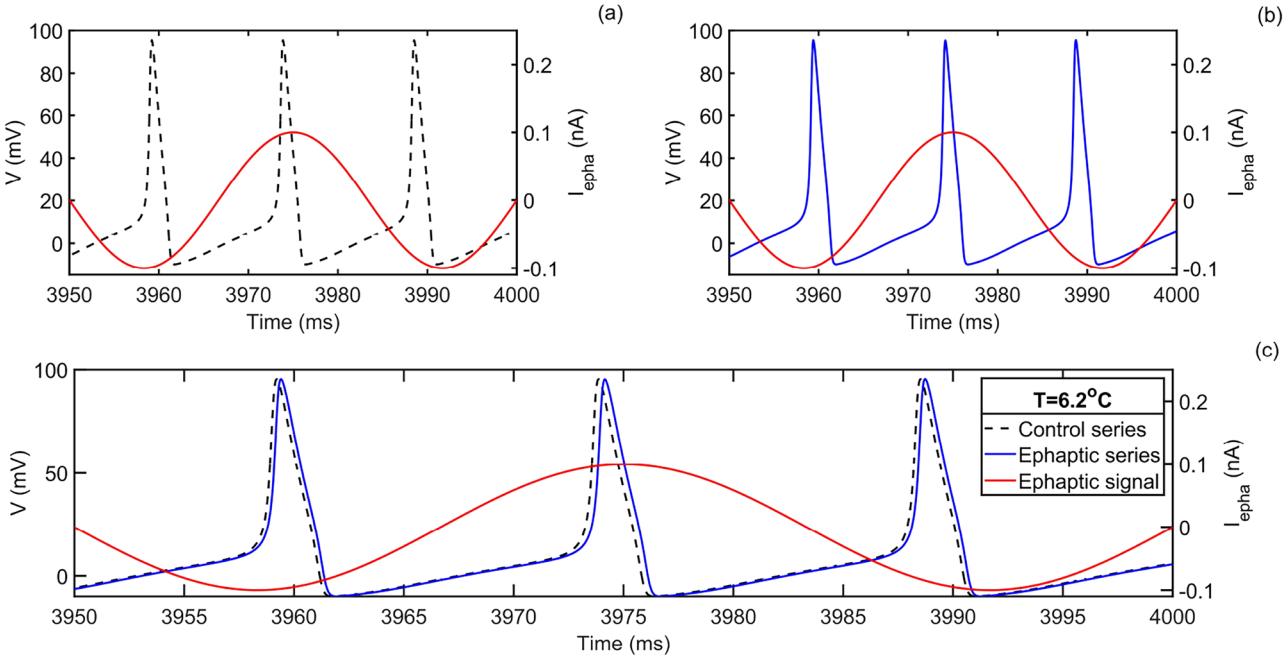

Figure 5. Comparison between control and ephaptic time series for injected current and ephaptic current equal to 10 μA and 100 nA. The figure compares the control time series ($I_{ephap} = 0$) and ephaptic time series ($I_{ephap} \neq 0$) obtained at the standard temperature $T = 6.2$ °C. Panel (**a**) displays the control membrane potential time series (black dashed line) and the ephaptic signal (red line) with frequency of 30 Hz in the absence of interaction between these signals. Panel (**b**) shows the ephaptic time series (blue line) along with the ephaptic signal ($f = 30$ Hz). Panel (**c**) presents the comparison between the control time series and the ephaptic time series, highlighting a small shift between the curves.

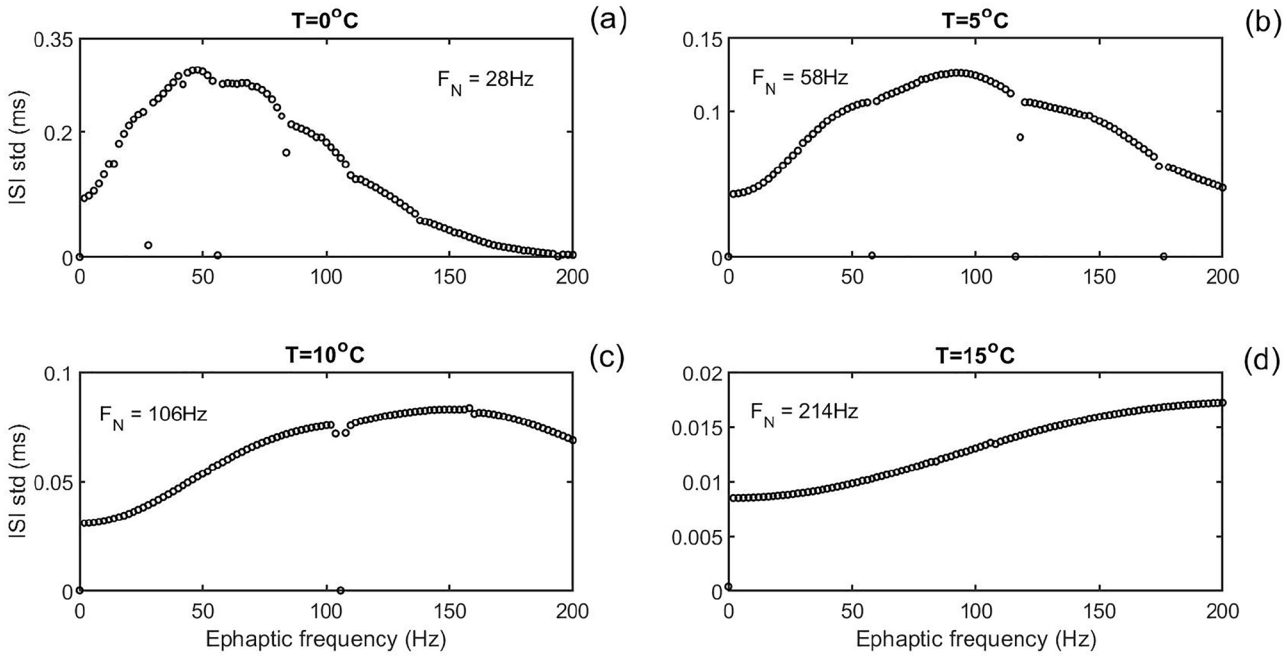

Figure 6. ISI standard deviation (ISI_{std}) versus ephaptic frequency oscillation for distinct temperatures. In (**a**) it is showed the standard deviation profile (ISI_{std}) for $T = 0$ °C and a minimum firing inject current ($I_0 \approx 9$ μA). In this figure is showed that model oscillates with natural (resonant) frequency of $f_N = 58$ Hz. Also, it is observed that ephaptic frequency values next to harmonics (27 Hz and 54 Hz for example) of natural frequency, the results of ISI_{std} tends to zero. In (**b**), for $T = 5$ °C and $I_0 \approx 10$ μA, the model presents a natural frequency $f_N = 58$ Hz. Similar to (**b**), the values of ISI_{std} tends to zero the natural frequency. In (**c**) and (**d**) it is shown the same kind of behavior as observed in (**a**) and (**b**) for the *ISIstd*. For $T = 10$ °C ($I_0 \approx 11$ μA) and $T = 15$ °C ($I_0 \approx 17$ μA) the model natural frequency are 214 Hz and 463 Hz, respectively. Additionally, it is shown in the figures that as T increases, the standard deviation of the ISI tends to decrease.

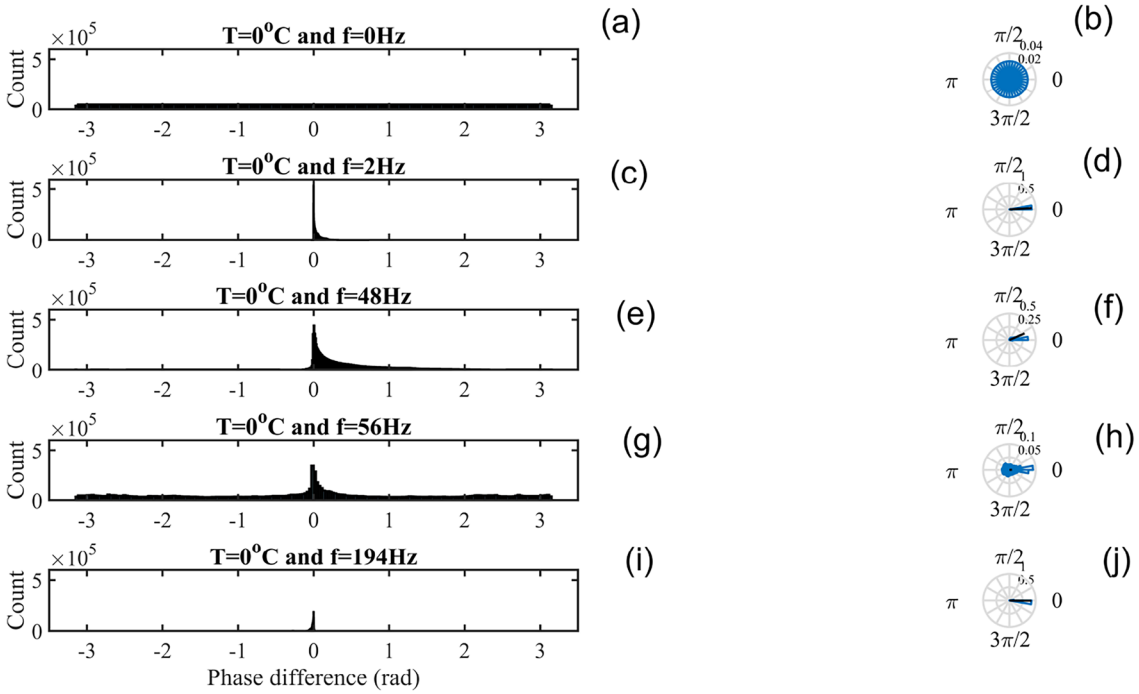

Figure 7. Phase difference between suprathreshold membrane potential and ephaptic signal for various ephaptic frequency values f at $T = 0$ °C. This figure illustrates how the phase difference between the suprathreshold membrane potential and ephaptic signal varies with changes in ephaptic frequency f. In (**a**), it is observed that for $T = 0$ °C and $f = 0$ Hz, the phase difference exhibits a flat distribution. Panel (**b**) presents the same result as in (**a**) using circular statistics. Panel (**c**) shows the phase difference for $T = 0$ °C and $f = 2$ Hz. Panel (**d**) displays the same result as in (**c**) for a circular plot. Panel (**e**) presents the phase difference distribution for $T = 0$ °C and $f = 48$ Hz using a histogram, and (**f**) shows the same data in a circular plot. Panel (**g**) and (**h**) depict the phase difference distribution and circular plot for $T = 0$ °C and $f = 56$ Hz. Panels (**i**) and (**j**) show the histogram and circular plot for the phase difference at $T = 0$ °C and $f = 194$ Hz.

distribution in circular plots for $f = 2$ Hz and $f = 48$ Hz. In Fig. 7g, for $f = 56$ Hz, the phase distribution is spread around the mean value ($\Delta\theta = 0°$), as shown in the corresponding circular plot (Fig. 7h). Finally, in Fig. 7i,j for $f = 194$ Hz, the phase difference peaks around $\Delta\theta = 0°$, though the angles are spread across negative phase difference values.

Discussion

This study explores the impact of temperature changes on neuronal ephaptic communication. The analysis begins by employing the Arrhenius Q_{10} approach to adapt the Hodgkin–Huxley model[24,34,41,42] to thermal variations. Furthermore, we adopt a methodology similar to previous empirical[38] and theoretical (hybrid model[11]) works, which discuss the implications of ephaptic communication in both subthreshold and suprathreshold neuronal regimes. The study reveals that ephaptic effects, such as ephaptic entrainment, can be significantly altered by temperature changes. Depending on the ephaptic signal frequency f and temperature T, scenarios previously identified as ephaptic entrainment may undergo abrupt changes, transitioning into non-entrainment scenarios. One significant finding of this study is the observed increase in firing rate and decrease in action potential amplitude with temperature variations (ephaptic off), which intuitively aligns with expectations. Additionally, our study analyzes the phase relationship between the input ephaptic current and neuronal firing, the interaction between the natural frequency of the HH-E model and harmonic frequencies, and the fluctuation of neuronal firing rates.

In the subthreshold regime, we studied the phase difference between the ephaptic signal I_{epha} and the membrane potential V_m while varying the frequency of the ephaptic signal and temperature. It was observed that the intensity of the phase difference tends to increase in the temperature range [0 °C–10 °C]. Additionally, we found that the frequency of the external ephaptic oscillation generally converges to an anti-phase regime ($\Delta\theta = \pi$) (Fig. 3). This anti-phase pattern is consistent with empirical results for cortical pyramidal neurons and hybrid models[10,11].

In the suprathreshold regime, temperature acts as a parameter capable of changing both spike frequency[68] and amplitude, as shown in Fig. 4. Figure 4 demonstrates that, as the firing rate increases with temperature (ranging from 0 to 15 °C), the minimum current I_0 necessary to trigger action potentials is also increased. Thus, the basal current I_0 that can initiate action potentials is modified with temperature changes. Consequently, based on the studied basal currents, we analyzed the relationship between the variation of the Inter-spike Interval (ISI), ephaptic frequency f, and temperature T. Moreover, in the suprathreshold regime, the addition of ephaptic interaction does not alter the firing rate (see Fig. 5), confirming that ephaptic interaction alone cannot induce spikes. The unique observed behavior in Fig. 5 is the phase shift caused by ephaptic interaction. This behavior

is also observed in empirical data[10] and the hybrid model[11]. Simulations focused on the suprathreshold regime (Fig. 6) illustrate the impact of including the ephaptic field on the fluctuation of ISI.

In the absence of ephaptic interaction ($f = 0$ Hz), Fig. 6a–d show that *ISIstd* remains close to zero regardless of temperature. However, the presence of an ephaptic field modifies *ISIstd* significantly, depending on both f and T. Specifically, in Fig. 6a, *ISIstd* increases abruptly and then returns to zero at high ephaptic frequencies f. This indicates that there are specific ephaptic frequencies where $ISIstd = 0$ or very close to zero. These frequencies correspond to points where the ephaptic frequency f matches the natural oscillation frequency F_N of the system or one of its harmonics, suggesting a resonance phenomenon. This resonance condition resembles the absence of ephaptic entrainment. Similar behavior is observed for other temperatures ($T = 5$ °C, 10 °C, and 15 °C). Another general observation from this figure is that *ISIstd* decreases approximately to zero as frequency increases. Here we can assume that ephaptic works like a low pass filter, acting more concisely at lower frequencies and having no effect at higher frequencies. Further, the ephapticity decreases the ISI std approximately tenfold as temperature increases (see at y-axis scales).

To further explore the effects of ephaptic interactions in the system, we selected specific ephaptic frequencies from Fig. 6a and applied the Hilbert transform to both membrane potential signals with and without the ephaptic signal. This approach allows us to extract the instantaneous phases of both signals and evaluate their phase difference, as shown in Fig. 7. Consistent with empirical findings[10], in the absence of ephaptic signal, the phase difference exhibits a flat distribution without a preferred phase (Fig. 7a,b). For non-resonant frequencies, such as $f = 2$ Hz (Fig. 7c), 48 Hz (Fig. 7e), and 194 Hz (Fig. 7i), the phase difference is centered around $\Delta\theta = 0$ with spread across positive and negative phase difference values. At resonant frequencies like $f = 56$ Hz (Fig. 7g), the phase difference is well-defined with angles spread around the mean. This analysis suggests that at non-zero *ISIstd*, the phase difference between membrane potential with and without ephaptic signal tends to increase. Conversely, at resonant frequencies (where $ISIstd \to 0$), the phase difference tends to exhibit a periodic pattern [see supplementary material]. The ephaptic signal serves as an oscillating electric field source that, according to Ohm's law, translates into the strength of the ionic current within the membrane, complementing other currents. This oscillating current component operates at a specific frequency near the neuron, inducing ephaptic entrainment characterized by a frequency preference, particularly when the ephaptic frequency closely aligns with or is harmonically related to the membrane's intrinsic frequency.

The development of ephaptic models represents a significant advance in recognizing the role of the ephaptic field in various brain functions, elevating ephaptic communication from its status as a secondary product to a central role[11,46]. Furthermore, considering the inclusion of temperature, the HH-E model could be extended. For instance, the addition of ionic channels whose activation is linked to temperature variations (thermo-TRP channels)[69–75]. The ephaptic models can transcend the traditional focus on synaptic communication, introducing ephaptic communication as an additional modulator in the complex neural scenario.

Considering ephaptic communication as a modulator[76,77], a new perspective opens up for understanding several brain processes. Not only does synapse, but also ephapticity emerge as a regulatory force capable of influencing neural dynamics in ways that were previously underestimated. Integrating ephaptic communication as an essential component provides a more holistic view of neural interactions and opens new opportunities for more in-depth investigations into the therapeutic and scientific implications of this less explored facet of neuronal communication, especially in pathological settings. Finally, our paper demonstrates that entrainment scenarios are modified by both the frequency of the ephaptic signal f and variations in temperature.

Data availability

The datasets generated during and/or analyzed during the current study are available from the corresponding author on reasonable request.

Received: 1 April 2024; Accepted: 20 August 2024
Published online: 29 August 2024

References

1. Park, K. S. Nervous system. In *Humans and Electricity: Understanding Body Electricity and Applications*, pp. 27–51 (Springer, 2023).
2. Studer-Luethi, B., Jaeggi, S. M., Buschkuehl, M. & Perrig, W. J. Influence of neuroticism and conscientiousness on working memory training outcome. *Pers. Individ. Differ.* **53**, 44–49 (2012).
3. Gathercole, S. E. The development of memory. *J. Child Psychol. Psychiatry Allied Discip.* **39**, 3–27 (1998).
4. Kandel, E. R. *et al. Principles of neural science* Vol. 4 (McGraw-hill, New York, 2000).
5. dos Santos Lima, G. Z. *et al.* Hippocampal and cortical communication around micro-arousals in slow-wave sleep. *Sci. Rep.* **9**, 5876 (2019).
6. Lima, G. D. S. *et al.* Mouse activity across time scales: Fractal scenarios. *PLoS ONE* **9**, e105092 (2014).
7. Katz & Schmitt. Eletric interaction between two adjacent nerve fibers. *J. Physiol.* 471–488 (1940).
8. Arvanitaky. Effects evoked in an axon by the activity of a contiguous one. *J. Physiol.* 91–108 (1942).
9. Hunt, T. & Jones, M. Fields or firings? Comparing the spike code and the electromagnetic field hypothesis. *Front. Psychol.* **14** (2023).
10. Anastassiou, C. A., Perin, R., Markram, H. & Koch, C. Ephaptic coupling of cortical neurons. *Nat. Neurosci.* **14**, 217–223 (2011).
11. Cunha, G. M., Corso, G., Miranda, J. G. V. & Dos Santos Lima, G. Z. Ephaptic entrainment in hybrid neuronal model. *Sci. Rep.* **12**, 1–10 (2022).
12. Jefferys, J. Nonsynaptic modulation of neuronal activity in the brain: Electric currents and extracellular ions. *Physiol. Rev.* **75**, 689–723 (1995).
13. Francis, J. T., Gluckman, B. J. & Schiff, S. J. Sensitivity of neurons to weak electric fields. *J. Neurosci.* **23**, 7255–7261 (2003).
14. Qiu, C., Shivacharan, R. S., Zhang, M. & Durand, D. M. Can neural activity propagate by endogenous electrical field?. *J. Neurosci.* **35**, 15800–15811 (2015).
15. Fröhlich, F. & McCormick, D. A. Endogenous electric fields may guide neocortical network activity. *Neuron* **67**, 129–143 (2010).
16. Anastassiou, C. A. & Koch, C. Ephaptic coupling to endogenous electric field activity: Why bother?. *Curr. Opin. Neurobiol.* **31**, 95–103 (2015).

17. Pinotsis, D. A. & Miller, E. K. In vivo ephaptic coupling allows memory network formation. *Cereb. Cortex* **33**, 9877–9895 (2023).
18. Bassett, D. S., Brown, J. A., Deshpande, V., Carlson, J. M. & Grafton, S. T. Conserved and variable architecture of human white matter connectivity. *Neuroimage* **54**, 1262–1279 (2011).
19. Han, K.-S. *et al.* Ephaptic coupling promotes synchronous firing of cerebellar purkinje cells. *Neuron* **100**, 564–578 (2018).
20. Queenan, B. N., Ryan, T. J., Gazzaniga, M. S. & Gallistel, C. R. On the research of time past: The hunt for the substrate of memory. *Ann. N. Y. Acad. Sci.* **1396**, 108–125 (2017).
21. Hedrick, T. & Waters, J. Effect of temperature on spiking patterns of neocortical layer 2/3 and layer 6 pyramidal neurons. *Front. Neural Circ.* **6**, 28 (2012).
22. Yu, Y., Hill, A. P. & McCormick, D. A. Warm body temperature facilitates energy efficient cortical action potentials. *PLoS Comput. Biol.* **8**, e1002456 (2012).
23. Burek, M., Follmann, R. & Rosa, E. Temperature effects on neuronal firing rates and tonic-to-bursting transitions. *Biosystems* **180**, 1–6 (2019).
24. Hodgkin, A. L. & Huxley, A. F. A quantitative description of membrane current and its application to conduction and excitation in nerve. *J. Physiol.* **117**, 500 (1952).
25. Moore, J. Temperature and drug effects on squid axon membrane ion conductances. In *Federation proceedings*, pp. 113 (Federation Amer Soc Exp Biol 9650 Rockville pike, Bethesda, MD 20814-3998, 1958).
26. Cao, X.-J. & Oertel, D. Temperature affects voltage-sensitive conductances differentially in octopus cells of the mammalian cochlear nucleus. *J. Neurophysiol.* **94**, 821–832 (2005).
27. Forrest, M. D. Can the thermodynamic Hodgkin–Huxley model of voltage-dependent conductance extrapolate for temperature?. *Computation* **2**, 47–60 (2014).
28. Tiwari, J. & Sikdar, S. Temperature-dependent conformational changes in a voltage-gated potassium channel. *Eur. Biophys. J.* **28**, 338–345 (1999).
29. Carpenter, D. O. Temperature effects on pacemaker generation, membrane potential, and critical firing threshold in aplysia neurons. *J. Gen. Physiol.* **50**, 1469–1484 (1967).
30. Ishiko, N. & Loewenstein, W. R. Effects of temperature on the generator and action potentials of a sense organ. *J. Gen. Physiol.* **45**, 105–124 (1961).
31. Ritchie, M. E. Reaction and diffusion thermodynamics explain optimal temperatures of biochemical reactions. *Sci. Rep.* **8**, 11105 (2018).
32. Rodríguez, B. M., Sigg, D. & Bezanilla, F. Voltage gating of shaker k+ channels: The effect of temperature on ionic and gating currents. *J. Gen. Physiol.* **112**, 223–242 (1998).
33. Liang, S. *et al.* Temperature-dependent activation of neurons by continuous near-infrared laser. *Cell Biochem. Biophys.* **53**, 33–42 (2009).
34. Hodgkin, A. L. & Huxley, A. F. Currents carried by sodium and potassium ions through the membrane of the giant axon of loligo. *J. Physiol.* **116**, 449–472 (1952).
35. Sjodin, R. & Mullins, L. Oscillatory behavior of the squid axon membrane potential. *J. Gen. Physiol.* **42**, 39–47 (1958).
36. Guttman, R. & with the technical assistance of Robert Barnhill. Temperature characteristics of excitation in space-clamped squid axons. *J. Gen. Physiol.* **49**, 1007–1018 (1966).
37. Hodgkin, A. & Huxley, A. Current and its application to conduction. *J. Physiol.* **117**, 500–544 (1952).
38. Anastassiou, C. A., Perin, R., Markram, H. & Koch, C. Ephaptic coupling of cortical neurons. *Nat. Neurosci.* **14**, 217 (2011).
39. Robertson, R. M. & Money, T. G. Temperature and neuronal circuit function: Compensation, tuning and tolerance. *Curr. Opin. Neurobiol.* **22**, 724–734 (2012).
40. Peleg, M., Normand, M. D. & Corradini, M. G. The arrhenius equation revisited. *Crit. Rev. Food Sci. Nutr.* **52**, 830–851 (2012).
41. Hodgkin, A. L. & Huxley, A. F. The components of membrane conductance in the giant axon of loligo. *J. Physiol.* **116**, 473–496 (1952).
42. Hodgkin, A. L., Huxley, A. F. & Katz, B. Measurement of current-voltage relations in the membrane of the giant axon of loligo. *J. Physiol.* **116**, 424–448 (1952).
43. Izhikevich, E. M. *Dynamical systems in neuroscience* (MIT press, London, 2007).
44. Han, K.-S. *et al.* Ephaptic coupling promotes synchronous firing of cerebellar purkinje cells. *Neuron* **100**, 564–578 (2018).
45. Schmidt, H., Hahn, G., Deco, G. & Knösche, T. R. Ephaptic coupling in white matter fibre bundles modulates axonal transmission delays. *PLoS Comput. Biol.* **17**, e1007858 (2021).
46. Cunha, G. M., Corso, G., Lima, M. M. & dos Santos Lima, G. Z. Electrophysiological damage to neuronal membrane alters ephaptic entrainment. *Sci. Rep.* **13**, 11974 (2023).
47. Binczak, S., Eilbeck, J. & Scott, A. C. Ephaptic coupling of myelinated nerve fibers. *Phys. D* **148**, 159–174 (2001).
48. Holt, G. R. & Koch, C. Electrical interactions via the extracellular potential near cell bodies. *J. Comput. Neurosci.* **6**, 169–184 (1999).
49. Goldwyn, J. H. & Rinzel, J. Neuronal coupling by endogenous electric fields: cable theory and applications to coincidence detector neurons in the auditory brain stem. *J. Neurophysiol.* **115**, 2033–2051 (2016).
50. Mechler, F. & Victor, J. D. Dipole characterization of single neurons from their extracellular action potentials. *J. Comput. Neurosci.* **32**, 73–100 (2012).
51. Hodgkin, A. & Katz, B. The effect of temperature on the electrical activity of the giant axon of the squid. *J. Physiol.* **109**, 240 (1949).
52. Fohlmeister, J. F. Voltage gating by molecular subunits of na+ and k+ ion channels: higher-dimensional cubic kinetics, rate constants, and temperature. *J. Neurophysiol.* **113**, 3759–3777 (2015).
53. Rosen, A. D. Nonlinear temperature modulation of sodium channel kinetics in gh3 cells. *Biochim. Biophys. Acta (BBA) Biomembranes* **1511**, 391–396. https://doi.org/10.1016/S0005-2736(01)00301-7 (2001).
54. Pahlavan, B., Buitrago, N. & Santamaria, F. Macromolecular rate theory explains the temperature dependence of membrane conductance kinetics. *Biophys. J* . **122**, 522–532 (2023).
55. Arrhenius, S. Über die dissociationswärme und den einfluss der temperatur auf den dissociationsgrad der elektrolyte. *Z. Phys. Chem.* **4**, 96–116 (1889).
56. Laidler, K. J. & King, M. C. The development of transition-state theory. *J. Phys. Chem.* **87**, 2657–2664 (1983).
57. Mardia, K. V. *Statistics of directional data* (Academic press, USA, 1972).
58. Berens, P. *et al.* Circstat: A matlab toolbox for circular statistics. *J. Stat. Softw.* **31**, 1–21 (2009).
59. Georgopoulos, A. P., Kalaska, J. F., Caminiti, R. & Massey, J. T. On the relations between the direction of two-dimensional arm movements and cell discharge in primate motor cortex. *J. Neurosci.* **2**, 1527–1537 (1982).
60. Georgopoulos, A. P., Schwartz, A. B. & Kettner, R. E. Neuronal population coding of movement direction. *Science* **233**, 1416–1419 (1986).
61. Oppenheim, A. V. *Discrete-time signal processing* (Pearson Education, India, 1999).
62. Dayan, P. & Abbott, L. F. *Theoretical neuroscience: Computational and mathematical modeling of neural systems* (MIT press, London, 2005).
63. Takens, F. Detecting strange attractors in turbulence. In *Dynamical Systems and Turbulence, Warwick 1980: proceedings of a symposium held at the University of Warwick 1979/80*, pp. 366–381 (Springer, 2006).
64. Sauer, T. Interspike interval embedding of chaotic signals. *Chaos Interdiscip. J. Nonlinear Sci.* **5**, 127–132 (1995).

65. Snider, R., Kabara, J., Roig, B. & Bonds, A. Burst firing and modulation of functional connectivity in cat striate cortex. *J. Neurophysiol.* **80**, 730–744 (1998).
66. Reich, D. S., Mechler, F., Purpura, K. P. & Victor, J. D. Interspike intervals, receptive fields, and information encoding in primary visual cortex. *J. Neurosci.* **20**, 1964–1974 (2000).
67. Kim, Y. & Panda, P. Visual explanations from spiking neural networks using inter-spike intervals. *Sci. Rep.* **11**, 19037 (2021).
68. Thompson, S. M., Masukawa, L. M. & Prince, D. A. Temperature dependence of intrinsic membrane properties and synaptic potentials in hippocampal ca1 neurons in vitro. *J. Neurosci.* **5**, 817–824 (1985).
69. Ito, E., Ikemoto, Y. & Yoshioka, T. Thermodynamic implications of high q10 of thermotrp channels in living cells. *Biophysics* **11**, 33–38 (2015).
70. Patapoutian, A., Peier, A. M., Story, G. M. & Viswanath, V. Thermotrp channels and beyond: mechanisms of temperature sensation. *Nat. Rev. Neurosci.* **4**, 529–539 (2003).
71. Kashio, M. & Tominaga, M. Trp channels in thermosensation. *Curr. Opin. Neurobiol.* **75**, 102591 (2022).
72. Avila, J., Lucas, J. J., Perez, M. & Hernandez, F. Role of tau protein in both physiological and pathological conditions. *Physiol. Rev.* (2004).
73. dos Santos Lima, G. Z. *et al.* Disruption of neocortical synchronisation during slow-wave sleep in the rotenone model of Parkinson's disease. *J. Sleep Res.* e13170 (2020).
74. Lima, M. M., Targa, A. D., dos Santos Lima, G. Z., Cavarsan, C. F. & Torterolo, P. Macro and micro-sleep dysfunctions as translational biomarkers for parkinson's disease. *Int. Rev. Neurobiol.* (2023).
75. Kandel, E. R. & al. et. *Princípios de Neurociências* (artmed, Porto Alegre, 2014), 5 edn.
76. Ruffini, G. *et al.* Realistic modeling of mesoscopic ephaptic coupling in the human brain. *PLoS Comput. Biol.* **16**, e1007923 (2020).
77. Vroman, R., Klaassen, L. J. & Kamermans, M. Ephaptic communication in the vertebrate retina. *Front. Hum. Neurosci.* **7**, 612 (2013).

Acknowledgements

MPBS is recipient of the Coordenação de Aperfeiçoamento de Pessoal de Nível Superior (CAPES - Brazil) fellowship (#88887.900715/2023-00) and fellowship #314906/2023-1. GZDL also is supported by Coordenação de Aperfeiçoamento de Pessoal de Nível Superior (CAPES/PRINT - Brazil) fellowship (#88887.877815/2023-00).

Author contributions

M.P.B.S. conceived the code model and results, G.M.C, G.C. and G.Z.S.L analyzed the results. All authors wrote and reviewed the manuscript.

Competing interests

The authors declare no competing interests.

Additional information

Correspondence and requests for materials should be addressed to G.Z.S.L.

Reprints and permissions information is available at www.nature.com/reprints.

Publisher's note Springer Nature remains neutral with regard to jurisdictional claims in published maps and institutional affiliations.